AAPS PharmSciTech, Vol. 12, No. 2, June 2011 (© 2011)
DOI: 10.1208/s12249-011-9623-0

Research Article

3D Simulation of Internal Tablet Strength During Tableting

Simo-Matti Siiriä,[1,3] Osmo Antikainen,[1] Jyrki Heinämäki,[1,2] and Jouko Yliruusi[1]

Received 21 December 2010; accepted 14 April 2011; published online 4 May 2011

Abstract. This study presents a new approach to model powder compression during tableting. The purpose of this study is to introduce a new discrete element simulation model for particle–particle bond formation during tablet compression. This model served as the basis for calculating tablet strength distribution during a compression cycle. Simulated results were compared with real tablets compressed from microcrystalline cellulose/theophylline pellets with various compression forces. Simulated and experimental compression forces increased similarly. Tablet-breaking forces increased with the calculated strengths obtained from the simulations. The calculated bond strength distribution inside the tablets showed features similar to those of the density and pressure distributions in the literature. However, the bond strength distributions at the center of the tablets varied considerably between individual tablets.

KEY WORDS: bonding; breaking strength; compaction; simulation; tableting.

INTRODUCTION

Pharmaceutical tablets are not generally compressed directly from powders. Instead, they are compressed from large particles, such as granules or pellets produced with various granulation techniques.

Tablet compression is a complicated process. First, the randomly packed particles are rearranged in a more compact order in a die. After and partly during this rearrangement, the particles also begin to deform. Particle deformations are commonly divided into three separate phenomena: elastic and plastic deformation, and fragmentation (1).

These compression deformations are separated into three distinct phases (2,3). The first phase is elastic deformation. During this phase, the particles behave like ideal elastic bodies: the particle deformation is considered reversible, rubber-like, and elastic. The second phase consists of plastic deformation, specifically irreversible plastic deformation. The last phase is fragmentation, or irreversible particle breakage, when high pressure overcomes the bonds binding particles together. These phases do not necessarily follow each other in order; in inhomogeneous tablet compression, where various particles are under different stresses and experience various shears, all phenomena can occur simultaneously.

The tablet compression process affects all main tablet characteristics, such as mechanical strength, porosity, wetting, and dissolution properties. Tablet strength is the sum of several factors: the primary factors are the bonding mechanism and the contact surface area of the bonds, and the secondary factors include particle shape, surface texture, and particle size (2).

Material behavior during tablet compression is often described with visco-elastic models, in which viscosity refers to plastic flow and the elasticity refers to ideal rubber-elastic behavior. The ratio of plastic and elastic behavior depends greatly on compression speed, which in pharmaceutical studies ranges from several milliseconds to several seconds.

Previous pharmaceutical studies have often classified materials as plastically deforming and fragmented materials (4–7). This classification, however, is quite problematic, as ideally fragmenting materials, such as sodium chloride, are often described as plastic. This misclassification is a natural result of the measuring environment. Monitoring punch pressures yields no data on individual particle rearrangement and fragmentation, but only a sum effect, which appears to be plastic.

In practice, directly measuring particle rearrangement or material behavior at particle–particle contact points during tableting is difficult. Consequently, the simulation modeling of tablet compression has generated growing interest.

Two basic simulation techniques are used in powder technology: the finite element method (FEM) and the discrete element method (DEM).

FEM models consider the powder a continuous mass. Rather than single particles, the FEM model tracks the movement of the powder between different areas of the simulated environment. The simulated environment is divided into portions; a large number of portions enhance the accuracy of the model, while lengthening the computing times. The rules of the model then determine how the mass can flow from one portion to another. As such, during

Electronic supplementary material The online version of this article (doi:10.1208/s12249-011-9623-0) contains supplementary material, which is available to authorized users.

[1] Division of Pharmaceutical Technology, Faculty of Pharmacy, University of Helsinki, P.O. Box 56 Viikinkaari 5 E FI-00014, Finland.
[2] Department of Pharmacy, Faculty of Medicine, University of Tartu, Nooruse 1, 50411 Tartu, Estonia.
[3] To whom correspondence should be addressed. (e-mail: simo.siiria@helsinki.fi)

development of the model, powder properties, such as flowability, become inputs for the model.

DEM models consider the powder one particle at a time. The particles move in the simulated area, and every collision between them is determined by the simulation. Since every particle is handled separately, the number of particles largely determines the computing time of the simulation. The rules of the model determine how the particles interact with each other. As such, during development of the model, the properties of single particles, such as friction and elasticity, become inputs for the model. Ketterhagen (8) has written an excellent review of DEM usage in the pharmaceutical industry.

Cunningham, Sinka, and others published two interesting papers on their FEM simulations of powder compaction. In the first (9), they use the model to determine the mechanical properties of microcrystalline cellulose. In the second (10), they studied the effect of lubrication on walls and the relative density inside the compaction. Khoei *et al.* introduced a software environment (11) to study powder compaction with a FEM model, which was further applied in a subsequent study (12).Wu *et al.* used a FEM model to study the tablet compression and density distribution during the compaction (13). They applied later (14) a FEM model to study the capping problem in tableting. Michrafy *et al.* (15) studied the relationship between wall friction and density distribution in tableting with a FEM model.

Chuan-Yu Wu studied the die-filling process with a 2D-DEM model (14). Samimi, Hassanpour, and others used the DEM models to study the compression of soft granules (16,17). In these studies, the authors applied the DEM to study how much the bulk behavior of the material correlates with its particle properties. Mehrotra *et al.* (18) used a DEM model to study the effect of cohesion and compression speed on the compression process. Sheng *et al.* used another DEM model in their study of the compaction process (19), which incorporated periodic boundaries in a unit cell. Another interesting study (20) introduced a 2D-DEM-FEM model, where every granule of the DEM model is further modeled with a FEM model. The model is used to study the compaction forces and particle deformation within tablet compression. The cracking behavior of agglomerates has been studied with DEM models (21–23).

Various DEM models have been used to study the strains during the compaction (16–19). There are theoretical models of the bond formation during tableting (24,25), but no studies applying DEM into analyzing the bond formation during the compaction exist. FEM models estimate the changes in the mass compacted (10–15), but due to their nature they cannot model inter-particulate bond formation.

The purpose of this study is to present a DEM-based simulation method that models 3D tablet compressions and takes into account the particle–particle bond formation during tablet compression. The advantages of this approach include obtaining a bond strength distribution in a tablet during and after a compression cycle. Also, the detailed information acquired from the bond locations can be further applied for example to study the formation of bonding network or cracking behavior of the tablets.

THEORY

Tablet Compression

In an eccentric tableting machine, the upper punch delivers the compression force which is usually defined as the maximum force experienced by the punches during the process. This force is measured from both the upper and the lower punches. The setup of the punch movements determines the final minimum distance between the two punches. This and the amount of material in the die essentially determine the compression force. In this study, the die was round (9 mm in diameter; Fig. 1) and both the upper and lower punches were round and flat-faced.

This study used a simplified approximation of bond forming. Simulated results are compared to real-life observations. In our approximation, each bond between particles is described as a potential forming between the particles. The maximum force a bond can sustain without breaking depends on the contact surface area between the particles. The surface

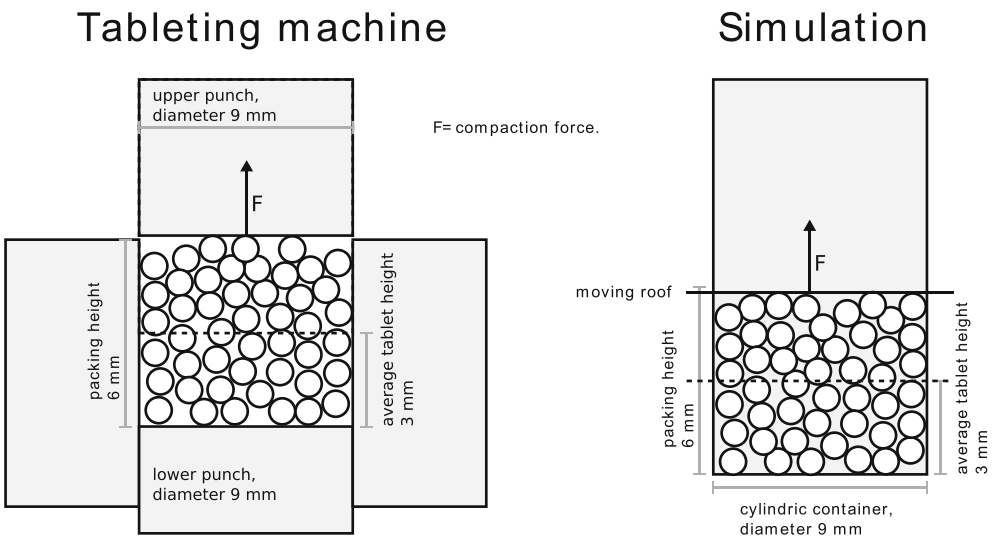

Fig. 1. Illustration of the tableting process. The compression force is defined as the maximum force needed to push the upper punch downwards

itself is a result of the force pressing the particles together. The strength of the tablet in our simulation results from the number and strength of the bonds formed during the compaction.

Simulation Environment

The simulation environment is based on our previous work (26), which describes it in detail. Briefly, the particles are modeled in a DEM system and are considered soft spheres in the simulation. The properties defined for each particle are location (x,y,z), radius, density, velocity (x,y,z), rotation (x,y,z), friction factor, elasticity, and stiffness. The forces included in the simulation are gravity, support forces between particles, support forces between the particles and the walls, and friction.

No system of more than two bodies can be solved completely, so some approximations are necessary to complete such simulations. The approach adopted here is to define the time as discrete steps of varying length. Every force and acceleration is assumed to remain constant during the time step. Smaller time steps result in a more accurate, but also more time-consuming simulation. Time step length varies so that when strong interactions occur (*e.g.*, collisions between particles), the time steps are smaller, and when weaker interactions occur (as in packing, when most of the particles are free of contacts), the time steps are longer. The rules for choosing the time step length are based on the highest speeds and changes in the force present in the previous time step. The limits for speeds, forces, and time steps have been optimized by trial and error in an attempt to obtain accurate simulations in a reasonable time.

In our previous work (26), the interaction between the particles was modeled as a spring force of the form $F=-k\Delta x$, where Δx is the overlapping distance of the particles, and k is a spring constant (in kilograms per square second). During packing and mixing, the interaction forces and overlapping distances are relatively small. During simulation of the powder compaction, the total density of the bulk roughly doubles. This compaction considerably increases both the interaction forces and particle overlapping. Under these conditions, the material stops behaving like an ideal spring. Instead, the force for further packing increases considerably faster as a function of the overlapping distance. The compaction curves from various attempts showed that a force of the form

$$F = -B'\left(k\Delta x + Ae^{a\Delta x} - A\right), \tag{1}$$

approximated the compaction well. Here, k, a, and A are constants determined by the properties of the material. Δx is the distance at which the two interacting particles overlap and is always positive or zero. $F(\Delta x)$ has been constructed so that $F(0)=0$. Particles have an elasticity factor B that determines how much energy is lost during a collision. When $B=1$, collisions are fully elastic and when $B=0$, the collisions are completely inelastic. When $B<1$, some energy will be lost in each collision. This is determined by multiplying F with B'. $B'=1$ when the particles move closer to each other during the collision. When the particles move away from each other, $B'=$B. This forces collision between the particles to lose a fraction of $(1-B)$ of its energy.

The approach adopted in these simulations is a simplified model of the actual particle deformation. In real life, particles tend to deform and break based on their physical properties, such as porosity. Many mechanical properties of pellets can be measured (27–30). In this study, our scope is to study the bond formation between particles in general without examining the effect of changing specific properties of the particles. As such, the particles are considered non-breaking, and their deformation is determined by letting the particles overlap each other as the compression increases. This deformation is sufficient to describe the inter-particle bond formation while keeping computational requirements negligible.

Compaction Forces

The time is divided into time steps. During each step, all forces are considered constant. The accuracy of the simulation thus strongly depends on the length of the time steps and the magnitude of the forces during each step. In our compaction experiments, the highest forces measured from the upper punch were of magnitude 10 kN, and the mass of the particles simulated was of magnitude 1 mg. In this type of situation, the momentary accelerations for a single particle can be very high. In real situations, these high accelerations vanish quickly as the particle moves away or is decelerated by other particles. Since the accelerations are constant during each individual time step, too long a time step can cause the particle to attain an unrealistic speed prior to the next step. This can force the particles to undergo oscillating acceleration, which accumulates energy inside the simulation. Applying a force of this magnitude to particles of this size slowed the simulations.

In order to acquire reasonable computation times, the resistance of the particles to compaction was reduced to 0.001 times the actual resistance. This reduced the compaction forces, the interaction forces between the particles, and thus the friction forces between them. Similarly, the force of gravity was also reduced, although the effect of gravity during compaction remained several magnitudes smaller than the other interactions, so the effect of the scaling of the gravity was minimal. This scaling softens the interactions between particles, thereby permitting the use of longer time steps. This reduced the computation times considerably. The relative densities of the tablets and the number of contact points and particle arrangements remain the same as if the original forces had been used.

Bond Approximations

A bond between particles can form when two particles overlap. If the force needed to keep particles overlapped exceeds a given constant F_{mb}, a new bond forms. This constant determines the minimum force needed to form a bond. F_{mb} must be large enough so that no bond forming occurs in normal particle collisions, but small enough so that the bonds begin to form towards the end of the particle rearrangement phase. After forming, the bond affects the particles, depending on their bond distance. The bond distance has three variables that are taken into account during the simulation:

- Current distance (R_c) is the distance between the centers of the two particles forming the bond.

- Relaxed distance (R_r) is the distance between the center of the particles at which the particles would cause 0 force on each other due to the bond.
- Bond-forming distance (R_f) is the distance at which the bond formed.

When a bond forms, R_r is derived from the R_f. If no external pressure is present, the bonds should relax. This relaxation is determined by a constant k_{rel}. When $k_{rel}=0$, no relaxation occurs. In such cases, the R_r of a bond is the same as that in which it formed. If $k_{rel}=1$, the bond will be completely relaxed, and the R_r will thus be R_1+R_2 regardless of the bond-forming distance (Fig. 2). The actual R_r for a given R_f is:

$$R_r = R_f + \big((R_1 + R_2) - R_f\big)k_{rel}, \tag{2}$$

where R_1 and R_2 are the radii of the two particles. Figure 2 illustrates these different distances.

As long as a bond exists between two particles, they can no longer collide with each other, but can still induce a force on each other. The force that particles induce depends on whether the particles are being repelled apart or attracted. In other words, the force differs if $R_c<R_r$ or $R_c>R_r$.

When $R_c<R_r$, the bond repels the particles. To ensure that bond formation restricts particle overlap similarly than particle collisions, the force that the bond induces when $R_c<R_r$ should be equal to that given in Eq. 1.

The potential was made symmetric around distance R_r. When $R_c>R_r$, the force assumes a form similar to that when $R_c<R_r$:

$$F = k\Delta x_b + Ae^{a\Delta xb} - A. \tag{3}$$

Δx_b in Eq. 3 represents the difference between the bond's relaxed distance (R_r) and the current distance between the interacting particles (R_c). R_r is the equilibrium point of the potential. The force induced around R_r remained symmetrical, which means that $F(R_r+x)=-F(R_r-x)$ (where x is any reasonable change in distance). With simple mathematics, this yields for Δx_b the form $\Delta x_b=(R_c-R_r)+R_r$.

The potential in this form is still unacceptable, however. At distance R_r, a strong, instantaneous change in force would occur. This force could cause oscillation, which would increase the error in the simulation. To avoid heavy oscillation, the force potential around R_r should be continuous and zero for the two particles. In this study, this was resolved by adding a multiplier L to the force when $R_f<R_c<R_r+(R_r-R_f)$. L is defined as $L=|R_c-R_r|(R_r-R_f)^{-1}$. This multiplier gradually lowers to zero the force that the bond induces around R_r. The potential obtained appears in Fig. 3. As a result, the potential remains symmetrical, similar to the potential used with no bonds for the compression, and reaches a point of stability near R_r.

The bond can change in two different ways. The bond can break completely if the particles are dragged too strongly apart. The opposing case for breaking the bond is when the particles are pressed too strongly together. In this case, the bond will be reform with a shorter R_f.

Ideally, the R_f would be the shortest distance (R_c) that the particles forming the bond reach. However, each bond will continually oscillate slightly around the distance that the forces present indicate is its rest position. This would mean that during the compression, the particles would constantly be closer to each other than the bond-forming distance (R_f). If the R_f were always updated by these oscillations, the bond would end up being unrealistically small, even with only small, constant pressure. To avoid this problem, a minimum change for R_f is used. The value of R_f is updated when

$$R_c < B_{lim}(R_f) + (1 - B_{lim})(R_1 + R_2), \tag{4}$$

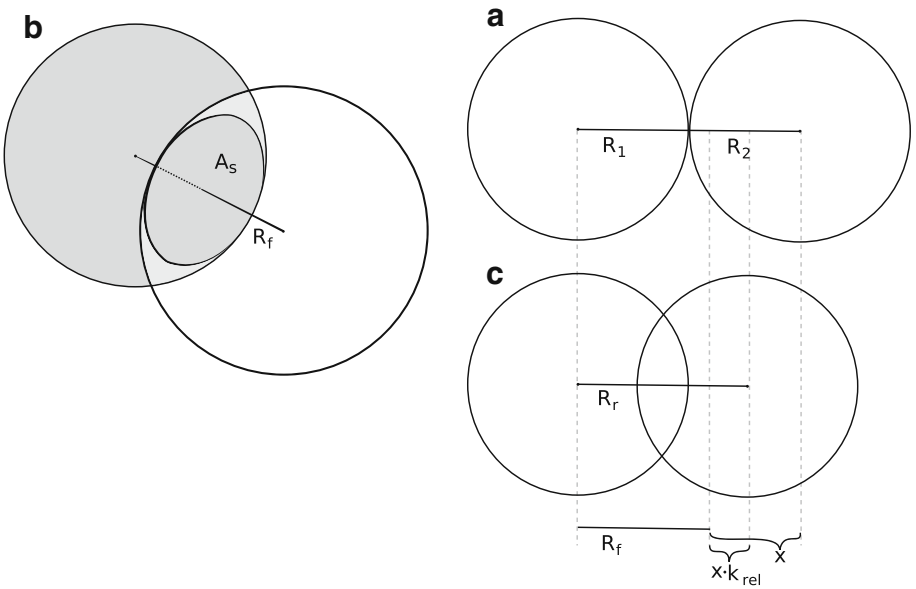

Fig. 2. Illustration of R_r, R_f, As, and k_{rel}. *A* shows two particles when they are barely in contact. This provides the maximum for bond length (R_1+R_2). *B* shows particles at the distance at which the bond forms. A_s is the gray area. *C* shows the particles after bond formation at a relaxed distance R_r. As is evident here, k_{rel} (see Eq. 2) determines the fraction at which the bond relaxes from its maximum. x in the figure shows the maximum relaxation. R_c indicates the current distance between two particles

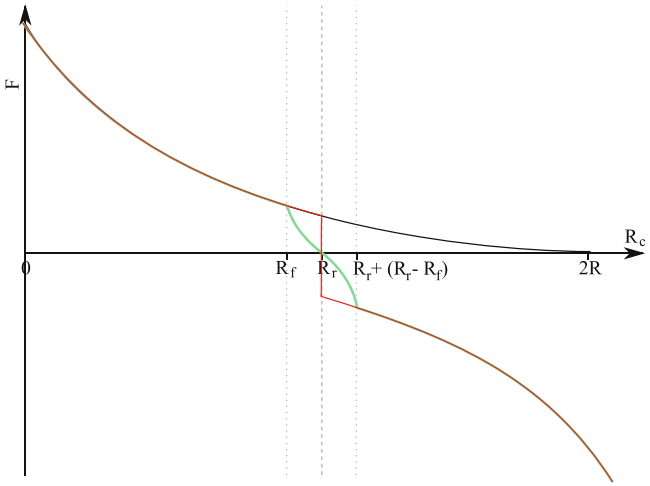

Fig. 3. Bond potential. The strong *black line* shows particle interaction without a bond, the *red line* shows the bond interaction without the scaling L, and the *green line* shows the final potential applied

where B_{lim} is a constant that determines the maximum R_c with the current R_f that will require the recalculation of the R_f. When $B_{lim}=1$, any R_c under the current R_f will suffice. When $B_{lim}=1.1$, the difference between R_1+R_2 and R_f must increase by 10% before recalculating R_f. The choice of B_{lim} is rather free; its absolute limits depend on the accuracy of the simulation. Too small a value will cause the bonds to shrink, due to random fluctuation, thus rendering the simulation unrealistic. On the other hand, the larger the value, the greater the difference between the two accepted lengths of the given bond. An excessively large B_{lim} would become the dominating factor in defining the bond relaxation distance rather than k_{rel}. This follows because a large B_{lim} would permit too much particle overlap without updating R_f and R_r. The R_r would thus remain larger than intended. Through trial and error, we determined a suitable value for B_{lim} of 1.05.

The breaking force for a bond is determined by the contact surface area (A_s) of the bond at its R_f (see Fig. 2) and the bonding coefficient K_b of the material. The breaking force of a bond is F_{BMax}, which appears in Eq. 5

$$F_{BMax} = K_b A_s, \tag{5}$$

where A_s is the contact surface area. If the force needed to keep the particles together (given in Eq. 3) exceeds F_{BMax}, the bond will break. At this point, the bond ceases to affect the interactions between particles. After this, the particles can again collide with each other. This may or may not later cause a new bond to form between the particles.

It should be noted that the A_s here should not be considered literally as the true contact area between the two particles, but as the geometric contact area. The true contact area between the particles depends on several factors, including the particle surface roughness and general texture (31–33). All material and particle properties affecting the strength of the bond formation are presented as a single value in these simulations. The K_b represents all the properties of a particle affecting its ability to form strong bonds.

Breaking Strength of a Tablet

The breaking strength of a tablet is usually determined through breaking experiments (34). In this procedure, the tablet is subjected to increasing diametral force. Once the tablet breaks, the force suddenly drops. The maximum force measured this way is called the tablet-breaking force. Tablet breaking usually begins from a crack on the middle axis of the tablet, and quickly propagates through the tablet.

The calculated strength S_t for a tablet was determined as

$$S_t = \sum_{n=1}^{N_b} \frac{F_{BMax_n}}{N}, \tag{6}$$

where N_b is the total number of bonds in the tablet, F_{BMax} is the breaking force of bond n, and N is the total number of particles. F_{BMaxn} describes the number and strength of bonds per particle in the tablet. Comparing the F_{BMaxn} of different tablets provides an estimate of their relative strengths.

The calculated strength (S_t) is a first approximation of the strength of a tablet, which does not take into account the method used to break the tablet. Essentially, S_t tells how strong the bonds per pellet are in the given tablet; a higher S_t indicates a stronger tablet. The literature describes several methods for determining the mechanical properties of the tablets (35). To determine the tablet strength in this study, we used the diametral test for tensile strength. When subjected to this test, the tablets generally break from the middle. As such, only a subset of the bonds actually determines the observed breaking strength. Breaking usually begins from one point, and the crack then propagates through the tablet. Tensile strength is a widely used method to determine tablet strength.

Bond Strength Distribution

The bond strength distribution represents the differences of average bond strengths within a certain volume. The bond strength distribution inside a tablet during compaction was determined from the simulations and was based on study of the strengths of individual bonds inside the tablet.

To determine the bond strength distribution in the tablet, the bond locations of each simulation series were transferred to cylindrical coordinates. In these, the positions of each bond were determined by its distance from the center and height from the bottom. The average strength of each *r*,*h* coordinate point was calculated based on the nearest bonds. Figures were then generated from the data. Because all the bonds with the same distance from the center share the *r* coordinate, more bonds are nearer the edges than the center (see video file 2 of the Electronic supplementary material (ESM)).

EXPERIMENTAL

Measurements

The composition of pellets was as follows: 50% (*w*/*w*) theophylline anhydrate (Ph. Eur.) and 50% (*w*/*w*) microcrystalline cellulose (Avicel PH-101, FMC International, Little Island, Cork, Ireland). Purified water was used as a granulation liquid. The pellets were made with the extrusion/spheronization technique (Nica M6L mixer/granulator; Nica

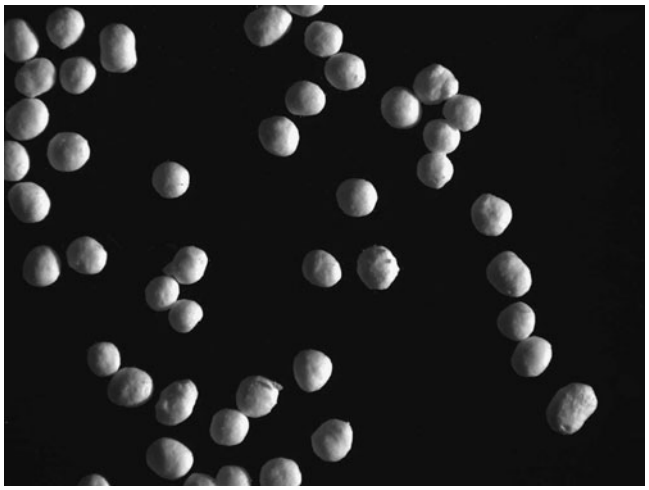

Fig. 4. Examples of the pellets studied

E170 extruder; Nica S320 spheronizer; Nica System AB, Mölndal, Sweden). In the granulator, the speed of the powder feeder was 35 rpm and the speed of the liquid input pump was 155 rpm. During extrusion, the speed of the extrusion head was 35 rpm, and that of the feeder, 45 rpm. The diameter of the apertures in the screen was 1.0 mm, the thickness was 1.25 mm, the spheronization speed was 900 rpm, and the spheronization time was at least 3 min. Pellets were dried for 24 h at room temperature (21±2°C). The dry pellets were sieved manually, and those between 0.7 and 1.0 mm in diameter were selected for subsequent experiments.

The pellets were generally round. The mean circularity, determined by an image analysis (calculated as in (36)) was 0.9±0.02. Based on the average size of the pellets and their weight, the density of the pellets was determined to be around 1.5 $g cm^{-3}$. Figure 4 shows examples of the pellets.

The tablets were compressed with an instrumented eccentric tableting machine (Korsch EK0, Erweka Apparatebau, Germany) using flat-faced punches with a diameter of 9 mm. The position of the lower punch was adjusted to exactly 7 mm below the surface of the die table. The compression speed was 10 rpm.

After the tablets were compressed, the strength of the tablet was determined in a breaking test. In this test, each of the tablets was subjected to increasing force until it broke. The development of the pressure as a function of time was recorded, as was the greatest force before the tablet broke. The results appear in Table I. The tablets were subjected to diametral stress between two metal jaws. These jaws moved at constant speed until the tablet broke.

The crushing strengths of the compressed tablets were measured with a Schleuniger-2E (Dr. K. Schleuniger & Co, Switzerland) tablet hardness tester.

The final set of test included a total of 16 tablets. Four different compression forces were used, and four tablets were made for each compression force. Because we did not intend to study the time dependency of the compaction, the compression speeds were lowered to an average of 500 ms. At such speeds, the elasticity of the material behaved identically in every compression.

In addition to the actual 16-tablet test set, we compressed another 20 tablets with parameters as identical as possible. This test set served to determine the average variation in tablet-breaking strength.

Simulations

The simulation series consisted of two distinct phases: packing and compression. The packing phase is similar to that used in our previous work (26). In short, a given number of particles is generated above the die. Based on their properties, these particles are dropped into the die. Frictional forces, rotation, and elasticity are taken into account during this process. Once all the particles are released and have settled, the simulation moves to the next phase. In total, 20 different packings were performed. All the calculations were performed in the 3D simulation software developed for this research.

The compression phase begins when packing ends. The upper punch moves in a sinusoidal curve, similar to the movement in a real eccentric tableting machine. An example of the packing and compression process is demonstrated in video file 1 of the ESM. The particles are described as soft spheres; so they overlap increasingly as the ceiling moves downwards. Bonds form when the force needed to keep them overlapped exceeds the given threshold. The contact surface area of the overlapping particles determines the strength of the bond (Fig. 2). To obtain four different compression forces, the initial height of the punch was set to four different values, and for each of these, the compression simulation was performed. Approximate tablet strength (S_t) was calculated after the compaction simulation. The movement of the upper punch was set separately for each group of four cases. The minimum distance between the upper and lower punches (which is also roughly the final tablet thickness) served as the reference for each series. The distances were 3.17, 3.25, 3.39, and 3.50 mm. The same distances were applied in both the simulations and experiments.

A density of 1.53 $g cm^{-3}$ was used in the simulations, because it gave approximately the correct bed height with the

Table I. Results Measured from the Tablet-Compaction and -Breaking Tests

Tablet thickness(mm)	Max F (kN)	Breaking force (N)	Tablet strength (relative)
3.50	9.1 ±0.34	22 ±4	5.7 ±1.0
3.39	9.6 ±0.36	29 ±5	7.4 ±1.3
3.25	12.9 ±0.30	51 ±8	13.1 ±2.05
3.17	14.8 ±0.33	53 ±7	13.8 ±1.7

Each series has four samples. Tablet strength (S_t) is a dimensionless value derived from the breaking strength to ease comparison with the simulated strength. It is scaled so that the mean strength of the values is 10

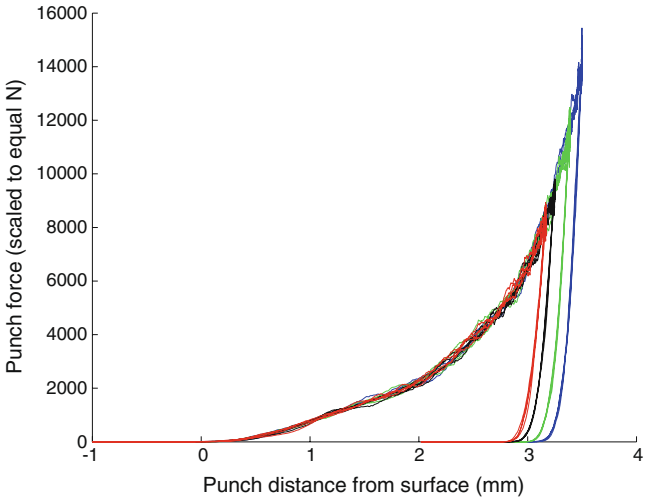

Fig. 5. Simulated compaction curves. The *red*, *black*, *green*, and *blue curves* indicate different compaction forces. The *red curves* show the lowest compaction force, and the *blue*, the highest

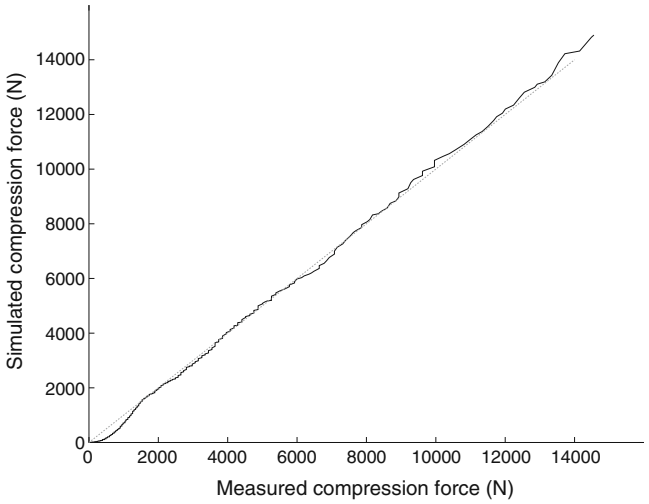

Fig. 7. The simulated compression force, as a function of the compression force measured is shown as a *black curve*. The *gray, dashed curve* shows the perfectly linear correlation

given mass of material. Assuming an average diameter of 0.855 mm, a density of 1.53 gcm^{-3}, and a spherical shape, 310 mg would be roughly equivalent to 616 particles. The height of the powder before compaction was set at 7.0 mm. In the final simulations, the friction coefficient between the particles was set to 0.3 and the parameters for interactions between the particles (see Eq. 1) were set as follows: k=900 Nm^{-1}, a=60000 m^{-1}, A=0.00032 N, and B=0.1.

In summary, the simulations were matched with the experiments based on identically sized die and punch, an identically high pellet pile at the start, identical punch movement, identical average size of the particles, and identical number of particles (approximating the number of particles with average size), identical density of the particles and finding the proper values for the particle interactions so that the measured compaction strengths match the simulated ones as closely as possible.

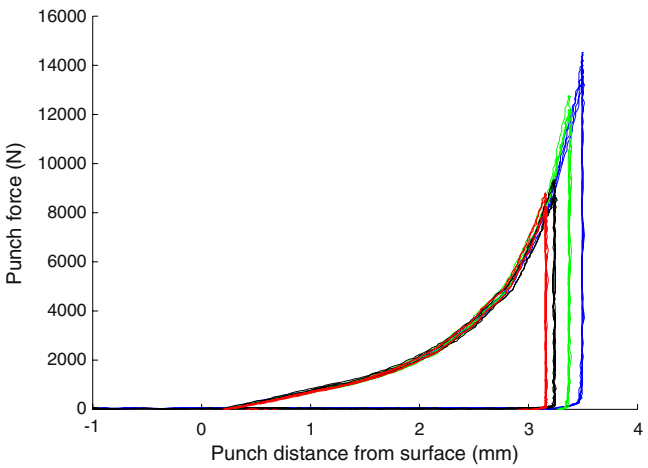

Fig. 6. Measured compaction curves. The *red*, *black*, *green*, and *blue curves* indicate different compaction forces. The *red curves* show the lowest compaction force, and the *blue*, the highest

RESULTS AND DISCUSSION

Compaction Forces

The simulated compression forces (Fig. 5) increased, as did the actual forces measured (Fig. 6). The compression force follows the function described in Eq. 1 in both simulations and measurements. Figure 7 shows the simulated compression force as a function of the compression force measured at a given distance. As is evident, both forces increase in very similar ways. At high compression speeds (typical of actual tablet compression), the equation becomes more complicated. At least one more exponential should be added, which takes into account the compaction speed.

Bond Strength Distribution

Bond formation during compaction was not linear as a function of the compression force, but rather sigmoidal (see Fig. 8). After the first bonds form, the speed increases until it begins to slow again. This slowing occurs because most neighboring particles have already bonded. Video file 2 of the ESM shows the locations of bonds that formed during compaction. Each point represents a bond. The color of the point indicates the strength of the bond; red represents the stronger bonds.

Figure 9 shows the bond strength distributions of the compressions with a tablet thickness of 3.17 mm. Images were mirrored along the center of the images. As is evident, edges always have a higher bond strength distribution than does the middle area. The top of the tablet seems nearly always to have a lower bond strength than does the rest of the tablet. The actual distribution of the bond strength in the middle area, however, seems to vary considerably between simulations. Sometimes the very center has a stronger area (Fig. 9, lower images) or the area might be moved aside from the actual center (Fig. 9, top right image). The center might also have an area of lower density (Fig. 9, left images). Video file 3 of the ESM shows the evolution of the bond strength

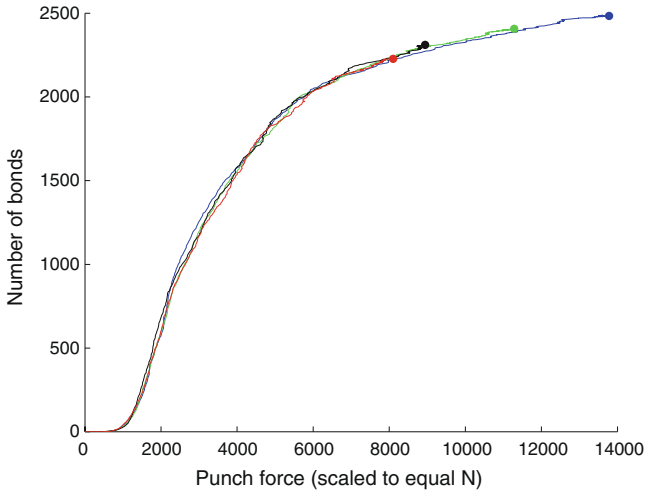

Fig. 8. Number of bonds as a function of compression force. Each curve is the average of four simulations with similar compression

distribution in the first example (Fig. 9, top left image). The video is scaled so that the height is constant. Note, however, that the tablet gets thins in the process.

Train (37) studied the pressure distribution inside tablets as early as 1957, showing different pressure distributions in various compression forces. All of his results showed some similarities. The highest pressures occurred at the top edges of the tablets, while the bottom edges experienced lower pressure than did the rest of the tablet. With stronger compression, the bottom middle area of the tablet showed an area of higher density, and the middle near the surface, an area of lower density. Macleod and Marshall (38) studied density distributions in ceramic uranium oxide. Their results showed dense areas near the walls and in the center. The weakest areas occurred on the bottom, as well as in the intermediate area between the edges and the center. They also noted that the tablet height/diameter ratio strongly affected the contrast of the density areas; with high ratios the differences were clearer. The authors varied the height/diameter ratios from ≈0.9 to ≈1.7. Eiliazadeh *et al.* (39) studied the density distribution inside variously shaped tablets, showing the density distributions for flat tablets with two compressions. Both compressions indicate high density on the top edges, weaker areas on the bottom edges, and a denser area in the middle of the tablet. This was more evident at higher pressure. The upper-center area was slightly less dense in both compressions. Frenning (40) performed a FEM simulation on tablet density distributions. His results also suggest that the strongest densities can be found on the top corners. The bottom corners also exhibited high density, as did most parts of the edges. The bottom middle area was also denser during compaction. In his work, the density was also modeled after unloading, which yielded a more evenly distributed density for the tablet.

In summary, previous studies suggest that the edges, especially the upper corners, are under stronger pressure than the rest of the tablet. Depending on the compression, the middle area of the tablet can have a clearly denser area, as well as another area that is even less dense than its surroundings (37). Our simulations showed similar behavior in the sense that the

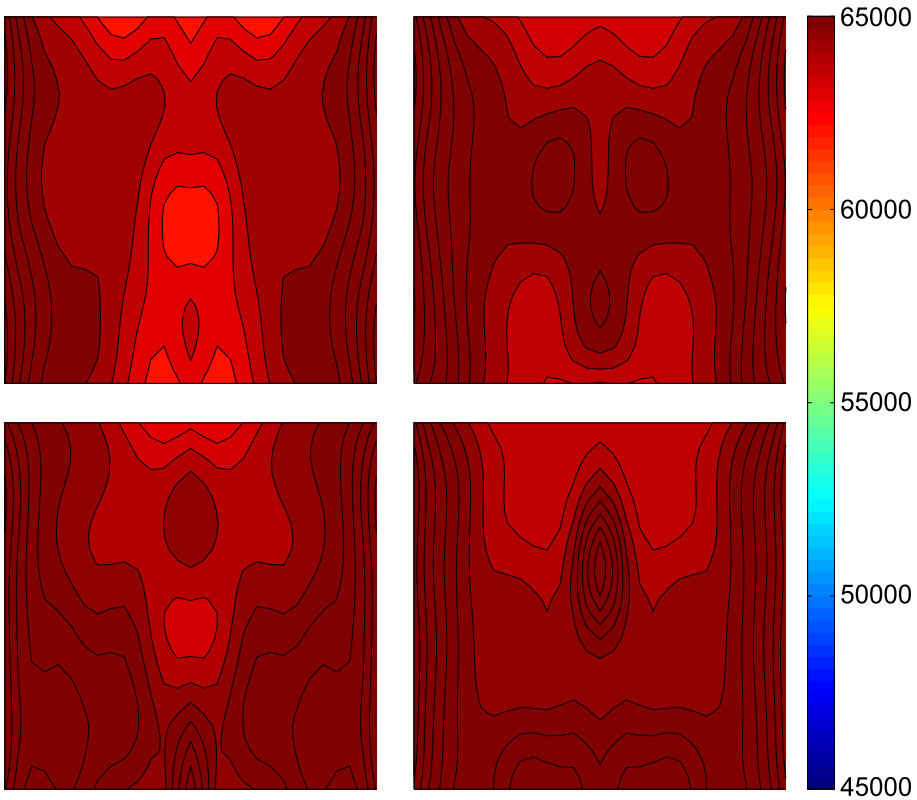

Fig. 9. Examples of the bond strength distributions of the simulated tablets. These distributions are obtained from the highest compression force, resulting in a tablet thickness of 3.17 mm. Images have been mirrored horizontally from the middle

Table II. Repeat Series for Both the Simulations and the Measurements

	Compression force (kN)	Breaking force (N)	%
Measured	14.4 ±0.530	53±8	17
	Compression force	Calculated strength	%
Simulated	14.9 ±0.420	10.8±0.05	0.5

Each series has 20 separate samples/simulations. Percentage (%) shows the standard deviation as a percentage of the actual strength

edges showed the highest bond strengths. Most of the simulations also showed an increase in bond strength in the middle of the tablets. In our case, no clear difference was evident between the corners of the edges and the rest of the sides. However, bond formation seemed to initiate generally from the upper corners, as is evident in video file 2 of the ESM. Clearer difference between the corners and the edges could not be seen probably because of the relatively small number of particles used and the low height/diameter ratio (around 0.3), which left little space for vertical variation.

Variation in Breaking Strength

The variation in the strength of the tablets was determined from both the simulations and the measurements. For the measurements, a test set of 20 tablets was measured with setups as identical as possible. The results of the measurements and the calculated strengths of a similar simulation series appear in Table II. The tablets measured usually broke in two halves from the center. Occasionally, the halves would still brake into several pieces.

The experimental breaking strengths varied more than the calculated strength of the simulated tablets. Calculated strength varies much less, because it is the sum of all the bonds in the tablet. Then again, the actual tablet breakage is the result of only some of the bonds in the tablet. Whether the variation in the tablet-breaking strengths was the result of actual deviation between the tablets or a reflection of the inhomogeneous inner character of each tablet remains uncertain. In theory, a significant portion of the observed variability in tablet-breaking strength may be attributed to the original orientation of a tablet in the breaking strength measurement. Tablet hardness probably varies considerably in various cutting and stressing directions, since the final tablet breaking occurs via the weakest bonds and slip planes.

As a rule of thumb, the standard deviation of tablet-breaking strength usually ranges from 5% to 15%. For example, Morisseau and Rhodes (41) observed ranges in standard deviation of 3.18% to 14.6%, and Krieger *et al.* (42) from 5.9% to over 10% in their tablet-breaking strength test. Similarly, Dahima *et al.* (43) recently reported a standard deviation of about 3-15% for their tablet-breaking strength.

Tablet Strengths as a Function of Compression Force

The tablet-breaking strengths measured appear in Table I, and calculated strengths (S_t) in Table III. The relative change in compression force as a function of punch movement increased similarly in both simulations and experiments.

Limitations

Particles are considered homogeneous from the inside. As such, any changes inside the particles are not considered in these simulations.

Because particles are considered ideal spheres, no real deformation is considered in these simulations. However, the particles do overlap each other considerably, which makes them behave as though they would deform into a hexagonal lattice (see video file 1 of the ESM for an illustration). Under extremely high compression, this approximation of particle formation would be unrealistic.

Particle deformation is considered plastic. No particle breakage is taken into account in the simulations, with the exception of the possibility of two bonded particles separating from each other again.

The breaking strength of the simulated tablet is approximated based on the total strength of the bonds within the tablet. While this method provides a comparable value for different tablets, it fails to take into account the internal distribution of the bond strengths. This is likely the reason for the much smaller variance in the calculated strength than in the measured breaking strengths.

CONCLUSIONS

This paper presents a new model for simulating bond formation during tableting.

The compaction force curves measured were nearly identical to those simulated. This indicates that the force function used in the bonds approximates well the situation observed.

The strength of the tablets was estimated based on the strength and number of the bonds formed during the compaction process. This increased as a function of the

Table III. Simulated Results for Different Compaction Strengths

Tablet thickness (mm)	Max F (relative)	Number of bonds	Strength (relative)
3.50	8.6 ±0.28	2,263 ±22	9.2 ±0.7
3.39	9.7 ±0.16	2,340 ±17	9.7 ±0.6
3.25	12.2 ±0.29	2,430 ±15	10.3 ±0.7
3.17	14.9 ±0.53	2,510 ±10	10.9 ±0.6

Each number is a mean value for four separate simulations ± standard deviation. The compaction force is relative. The calculated strength of the tablets (S_t) is a dimensionless value that shows the relative amount of bonding energy within each tablet. The number is scaled so that the mean strength of the simulation series is 10

compression force in the same way as the measured breaking strength did in the tablets measured.

The standard deviation in tablet-breaking strength was considerably greater than the standard deviation in the calculated strength of the simulations. This stems from the fact that only a fraction of the bonds that keeping the tablet together affects tablet tensile strength.

The bond strength distribution in the simulated tablets resembled in large scale the density distributions found in the literature. The area in the middle of the tablet, however, did vary considerably.

LIST OF SYMBOLS

A (N)	Is a constant that determines the magnitude of the exponential part of the interaction force between particles.
A (m^{-1})	Is a constant that determines how quickly the exponential part of the interaction force between particles increases with distance.
A_s (m)	Is the contact surface area of a given bond.
B (dimensionless)	Is a constant that determines the elasticity of the material. If $B=0$, the material is completely inelastic; if $B=1$, it is completely elastic.
B' (dimensionless)	Serves to obtain the elasticity of the interactions. $B'=1$ when particles are approaching each other. $B'=$B in any other situation.
B_{lim} (dimensionless)	Is a constant that determines how much further than R_f two particles must be compressed before the R_f for the bond between them must be recalculated (see Eq. 4).
F (N)	Is any given force in question.
F_{mb} (N)	Is the minimum force required to form a bond.
F_{BMax} (N)	Is the maximum force a given bond can bear before breaking.
K_b (N m^{-2})	Is the bonding coefficient of the given material. K_b describes how much force is needed for a bond of given area A to break.
K (kg m^{-2})	Is a spring constant; actual value depends on the material simulated.
k_{rel} (dimensionless)	Is a constant that describes how much a bond will relax from its R_f (See Eq. 2).
L (dimensionless)	Is a scaling factor used to obtain a bond force of zero near $R_r(1 \geq L \geq 0)$.
N (dimensionless)	Is the total number of particles.
N_b (dimensionless)	Is the total number of bonds.
R_c (m)	Denotes the current distance between two particles bound together.
R_f (m)	Denotes the bond-forming distance. This is the distance at which a bond is formed. It is unique for each bond and can change if the particles are further compressed.
R_r (m)	Or relaxed distance, is the distance between two particles in which the bond between them subjects no force on them.
R_1, R_2 (m)	Are the radii of the particles in question.
S_t (N, scaled dimensionless)	Is the calculated strength of a tablet (see Eq. 6).
t (s)	Time.
Δx (m)	Is the overlapping distance of two particles.
Δx_b (m)	Is the effective extent of the bond when stretched. $\Delta x_b=(R_c-R_r)+R_r$

REFERENCES

1. Santos HMM, Sousa JJMS. Pharmaceutical manufacturing handbook: production and processes. USA: Wiley; 2008.
2. Alderborn G, Nyström C. Pharmaceutical powder compaction technology. New York: Marcel Dekker; 1996.
3. Carstensen JT. Advanced pharmaceutical solids. New York: Marcel Dekker; 2001.
4. Morehead WT. Viscoelastic behavior of pharmaceutical materials during compaction. Drug Dev Ind Pharm. 1992;18(6–7):659–75.
5. Mitrevej A, Faroongsarng D, Sinchaipanid N. Compression behavior of spray dried rice starch. Int J Pharm. 1996;140(1):61–8.
6. Guo HX, Heinämäki J, Yliruusi J. Characterization of particle deformation during compression measured by confocal laser scanning microscopy. Int J Pharm. 1999;18(6–7):99–108.
7. Antikainen O, Yliruusi J. Determining the compression behavior of pharmaceutical powders from the force–distance compression profile. Int J Pharm. 2003;252(1–2):253–61.
8. Kettenhagen WR. Process modeling in the pharmaceutical industry using the discrete element method. J Pharm Sci. 2008;98(2):442–70.
9. Cunningham JC, Sinka IC, Zavaliangos A. Analysis of tablet compaction. I. Characterization of mechanical behavior of powder and powder/tooling friction. J Pharm Sci. 2004;93(8):2022–39.
10. Sinka IC, Cunningham JC, Zavaliangos A. Analysis of tablet compaction. II. Finite element analysis of density distribution in convex tablets. J Pharm Sci. 2004;93(8):2040–53.
11. Khoei AR. An integrated software environment for finite element simulation of powder compaction processes. Materials Processing Technology. 2002;130–131:168–74.
12. Khoei AR, Azami AR, Azizi S. Computation modeling of 3D powder compaction processes. Materials Processing Technology. 2007;185:166–72.
13. Wu CY, Bentham AC, Hancock BC, Best SM, Elliott JA. Modelling the mechanical behaviour of pharmaceutical powders during compaction. Powder Technol. 2005;152:107–17.
14. Wu CY, Hancock BC, Mills A, Bentham AC, Best SM, Elliot JA. Numerical and experimental investigation of capping mechanism during pharmaceutical tablet compaction. Powder Technol. 2008;181:121–29.
15. Michrafy A, Dodds JA, Kadiri MS. Wall friction in the compaction of pharmaceutical powders: measurement and effect on the density distribution. Powder Technol. 2004;148(1):53–5.
16. Hassanpour A, Ghadiri M. Distinct element analysis and experimental evaluation of the Heckel analysis of bulk powder compression. Powder Technol. 2004;141:251–61.
17. Samimi A, Hassanpour A, Ghadiri M. Single and bulk compression of soft granules: experimental study and DEM evaluation. Chem Eng Sci. 2005;60:3993–4004.
18. Mehrotra A, Chaudhuri B, Faqih A, Tomassone MS, Muzzio FJ. A modelling approach for understanding effects of powder flow

properties on tablet weight variability. Powder Technol. 2009;188:295–300.
19. Sheng Y, Lawrence CJ, Briscoe BJ. Numerical studies of uniaxial powder compaction process by 3D DEM. Eng comput. 2003;21 (2/3/4):304–17.
20. Procopio AT, Zavaliangos A. Simulation of multi-axial compaction of granular media from loose to high relative densities. J Mech Phys Solids. 2005;53:1523–51.
21. Golchert D, Moreno R, Ghadiri M, Litster J. Effect of granule morphology on breakage behaviour during compression. Powder Technol. 2004;143–144:84–96.
22. Antonyuk S, Palis S, Heinrich S. Breakage behaviour of agglomerates and crystals by static loading and impact. Powder Technol. 2011;206(1–2):88–98.
23. Khanal M, Schubert W, Tomas J. DEM simulation of diametral compression test on particle compounds. Granular Matter. 2005;7:83–90.
24. Hiestand EN. Tablet bond. I. A theoretical model. Int J Pharm. 1991;67:217–29.
25. Hiestand EN, Smith DP. Tablet bond. II. Experimental check of model. Int J Pharm. 1991;67:231–46.
26. Siiriä S, Yliruusi J. Particle packing simulations based on Newtonian mechanics. Powder Technol. 2007;174:82–92.
27. Johansson B, Wikberg M, Ek R, Alderborn G. Compression behaviour and compactability of microcrystalline cellulose pellets in relationship to their pore structure and mechanical properties. Int J Pharm. 1995;117(1):57–73.
28. Johansson B, Alderborn G. Degree of pellet deformation during compaction and its relationship to the tensile strength of tablets formed of microcrystalline cellulose pellets. Int J Pharm. 1996;132(1–2):207–20.
29. Salako M, Podczeck F, Newton JM. Investigations into the deformability and tensile strength of pellets. Int J Pharm. 1998;168(1):49–57.
30. Eriksson M, Alderborn G. The effect of particle fragmentation and deformation on the interparticulate bond formation process during powder compaction. Pharm Res. 1995;12:1031–9.
31. Nayak PR. Random process model of rough surfaces in plastic contact. Wear. 1973;26(3):305–33.
32. Podczeck F, Newton JM. The evaluation of a three-dimensional shape factor for the quantitative assessment of the sphericity and surface roughness of pellets. Int J Pharm. 1995;124(2):253–9.
33. Sebhatu T, Alderborn G. Relationships between the effective interparticulate contact area and the tensile strength of tablets of amorphous and crystalline lactose of varying particle size. Eur J Pharm Sci. 1999;8(4):235–42.
34. Stanley P. Mechanical strength testing of compacted powders. Int J Pharm. 2001;227(1–2):27–38.
35. Fell JT, Newton JM. Determination of tablet strength by the diametral-compression test. J Pharm Sci. 1970;59(5):688–91.
36. Hellen L, Yliruusi J. Process variables of instant granulator and spheroniser: III. Shape and shape distribution of pellets. Int J Pharm. 1993;96:217–23.
37. Train D. Transmission of forces through a powder mass during the process of pelleting. Trans Inst Chem Eng. 1957;35:258–66.
38. Macleod HM, Marshall K. The determination of density distributions in ceramic compacts using autoradiography. Powder Technol. 1977;16:107–22.
39. ElIiazadeh B, Briscoe BJ, Sheng Y. Investigating density distributions for tablets of different geometry during the compaction of pharmaceuticals. Part Sci Technol. 2003;21:303–16.
40. Frenning G. Analysis of pharmaceutical powder compaction using multiplicative hyperelasto-plastic theory. Powder Technol. 2007;172:103–12.
41. Morisseau KM, Rhodes CT. Near-infrared spectroscopy as a nondestructive alternative to conventional tablet hardness testing. Pharm Res. 1997;14:108–11.
42. Krieger M, Fähler FJ, Baumgartner K. Determination of tablet hardness with strain gauge equipped instruments. Drug Dev Ind Pharm. 1995;21(19):2201–12.
43. Dahima R, Pachori A, Netam S. Formulation and evaluation of mouth dissolving tablet containing amlodipine besylate solid dispersion. International Journal of ChemTech Research. 2010;2 (1):706–15.